Solder-Bonded Carbon Nanotube Thermal Interface Materials

Michael T. Barako, Yuan Gao, Amy M. Marconnet, Mehdi Asheghi, and Kenneth E. Goodson
Department of Mechanical Engineering
Stanford University
440 Escondido Mall
Stanford, CA 94305
Phone: (717)339-6794
Email: mbarako@stanford.edu

ABSTRACT

Vertically-aligned carbon nanotube (CNT) films offer an attractive combination of properties for thermal interface applications, specifically high thermal conductance and mechanical compliance. In this work, we examine the use of a solder bonding layer to attach and transfer CNT films from the silicon growth substrate onto metalized surfaces. Indium foil is considered as a bonding layer for low-temperature (<150°C) applications while a tin-plated aluminum/nickel foil is used for high temperature applications (<1000°C). The intrinsic thermal conductivity of the CNT film and the thermal boundary resistances between the CNT film and the surrounding materials are measured with comparative infrared microscopy before and after solder bonding. The thermal properties are measured over a range of applied compressive stress. In general, compressive stress reduces the thermal boundary resistance and improves the thermal conductivity of the CNT films. Solder bonding of the exposed (non-growth) interface reduces the thermal boundary resistance by up to a factor of 30 over a dry unbonded contact.

KEY WORDS: indium bonding, Nanofoil, infrared thermometry, thermal interface

NOMENCLATURE

dT/dx	temperature gradient [K/m]
k	thermal conductivity [W/m/K]
q"	heat flux [W/m^2]
R"	specific thermal resistance [mm^{2}K/W]

Greek symbols

ΔT	temperature difference [K]
σ	compressive stress [Pa]
τ	stress relaxation time constant [s]

Subscripts

final	mechanical equilibrium
FS	fused silica
int	interface
ref	reference layer

INTRODUCTION

Thermomechanical stresses arise in electronics and other thermal devices due to the mismatch between the coefficients of thermal expansion in the presence of large temperature gradients. These mechanical stresses often lead to failure of the thermal interface material (TIM). Carbon nanotube films have received much attention over the last decade owing to the high intrinsic thermal conductivity of individual CNTs [1]. This high axial thermal conductivity reduces the thermal resistance contribution of the bulk interface material, while the low transverse elastic modulus alleviates thermomechanical stresses [2, 3]. In addition, CNT films demonstrate viscoelastic stress relaxation, which is an attractive property for the mechanical stability of thermal interfaces. Stress relaxation allows the film to adjust and accommodate changes in strain due to temperature fluctuations. For a thermally conductive bulk TIM, the thermal boundary resistance between the CNT film and the substrate limits the overall thermal performance of these films [3, 4]. There is a need for a scalable, robust, and thermally-conductive bonding technique to implement these nanostructured films into practical applications.

Previous work has focused on improving the thermal conductivity of the intrinsic CNT film, which ranges from ~10^{-1} to ~10^{2} W/m/K [3, 5, 6]. These values represent a significant reduction from the axial thermal conductivities reported for individual CNTs, which can be as high as ~3500 W/m/K [1]. The thermal conductivity of CNT films is governed by the CNT volume fraction, chirality, defects, morphology, and CNT-CNT interactions [6-8]. Marginal improvements in CNT film thermal conductivity are possible using post-growth material modifications. This includes biaxial compression to increase the volume fraction, infiltration of the CNT film with a polymer or metal matrix to reduce air gaps, possibly improving the conduction between nanotubes [8, 9], and high temperature annealing to reduce the amount of amorphous carbon and repair sidewall defects [10]. As the intrinsic thermal conductivity of the CNT film improves, the interface resistances between the bulk CNT film and the surrounding materials become increasingly important. Metallic [5, 11], electrothermal [4], and thermocompressive [12-14] bonding techniques have been investigated to reduce the high CNT-substrate thermal boundary resistance.

To address the need for a scalable, robust, and thermally-conductive bonding technique, we transfer CNT films grown on a standard silicon wafer using a binder metal layer. This avoids the difficulties of growing CNT films directly onto a heat sink or other thermal device. The metal binder layer increases the thermal conductance of the CNT-device interface while preserving the high thermal conductivity and mechanical compliance of the bulk CNT TIM. In addition, this decouples the optimization of CNT film growth from the study of bonding techniques.

Indium solder has been successfully used in conventional electronics packaging applications for thermal management [15]. Thin (1μm) films of evaporated indium have been used to bond metalized CNT films to adjacent surfaces to reduce the contact resistance at the interface [5]. The low melting

temperature of indium (156.6°C) requires that the indium-bonded interfaces remain below this operating temperature. In this manuscript, we employ both an indium thin film binder and a commercial nanostructured Al/Ni film which can be processed at low temperatures but remains stable at high temperatures. Comparative infrared thermometry is used to measure the intrinsic thermal conductivity of the CNT film and the thermal boundary resistances between the CNT film and the surrounding materials. The CNT film boundary resistance is measured before and after bonding. The thermal properties are measured over a range of applied out-of-plane compressive strain. The viscoelastic stress response of the CNT film to applied strain is also characterized, including the relaxation time constant.

EXPERIMENTAL METHODS

Sample Preparation

Vertically-aligned multi-wall CNT films (see Figure 1) are grown by chemical vapor deposition on silicon substrates (Nanostructured & Amorphous Materials, Inc.). These films are 500 μm-thick and the individual tubes have an inner diameter of 5-8 nm and an outer diameter of 7-10 nm. The density of the films is approximately 10^{10}-10^{11} CNT/cm^2. The CNT films and fused silica (FS) substrates are coated with 50 nm chromium, 20 nm nickel, and 150 nm gold using e-beam evaporation. The gold layer is the active bonding surface to weld to the solder layer. The nickel layer prevents the diffusion of gold atoms and the chromium layer serves as an adhesion layer. The metallization of the bonded surfaces enables thermally conductive metal-metal solder bonding instead.

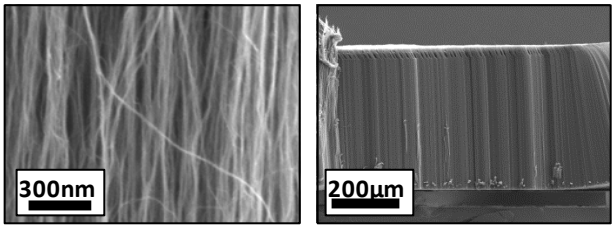

(a) (b)

Fig. 1: (a) Scanning electron micrograph (SEM) showing vertical alignment of individual CNTs within the film. (b) SEM of an un-bonded 500 μm-thick vertically-aligned CNT film.

Indium has been an attractive bonding material for electronics packaging, adhering well to gold-plated surfaces with the aid of solder flux [15]. In general, the bonding layer should be as thin as possible to reduce the thermal resistance across this layer. In this work, 25 μm-thick indium foil (Indium Co.) is used. However, it would be possible to obtain a thinner layer by evaporating the indium layer directly onto the surface. The indium foil is cleaned with acetone and deionized water and coated with a thin layer of solder flux (Indium Co., Flux 5R). The foil is then placed between the CNT film and the fused silica substrate, and the stack is heated on a hot plate to 180°C. Light pressure is applied (~100 kPa) to ensure good contact and wetting of the indium to the gold surfaces. The indium melts and bonds the gold surface on the CNT film to the gold surface on the fused silica substrate, as shown in Fig. 2a.

To investigate its suitability as a high temperature stable bonding layer for CNT-based TIMs, Nanofoil® (NF) (Indium Co.), a Sn-plated Al/Ni superlattice film, is used to bind the Cr/Ni/Au coated CNT film to a FS substrate. The materials which compose the NF binding layer have the additional benefits of abundance and non-toxicity. When ignited, the Al/Ni layers alloy in an exothermic reaction to provide highly localized heating up to 1500°C over a very short time period (~10 ms). This reaction melts the Sn-plating, welding the Sn to the adjacent Au surfaces (see Figure 3) and the Sn-Au bond is stable up to 1000°C. The high temperatures associated with alloying are isolated to the interface due to the short time of the reaction. This technique demonstrates promise as a simple, scalable process for bonding CNT-based and other nanostructured TIMs.

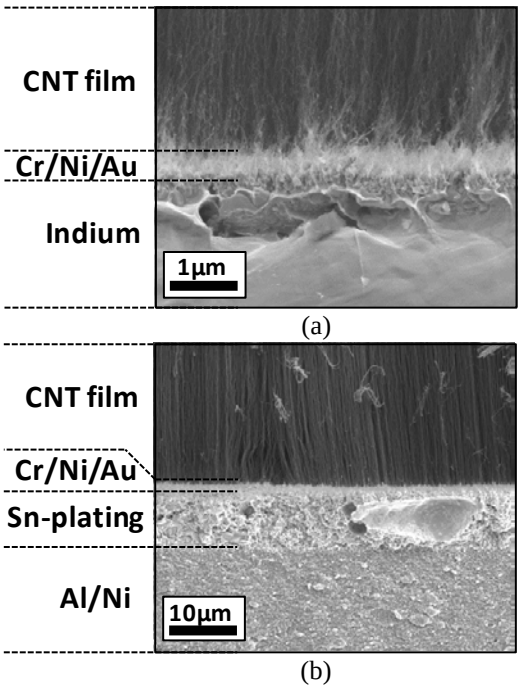

(a)

(b)

Fig. 2: (a) SEM of indium foil soldered to a metalized CNT film and (b) SEM of NF with Sn-plating welded to a metalized CNT film.

The Nanofoil is placed between the metalized CNT surface and the metalized fused silica substrate. The thermal boundary resistance is measured at the interface ("un-bonded" data) prior to reacting the NF. The NF behaves as a thin metallic layer in dry contact with the CNT film and the fused silica substrate. As a result, the thermal boundary resistance is very large (~10^3 mm^2 K/W). To bond the surfaces, ~100 kPa pressure is applied to ensure good contact between the gold surfaces and the Sn-plating. The NF is ignited with a localized heat pulse that initiates the reaction of the entire layer. The reaction lasts for ~1ms and the sample remains cool, since this reaction has a high energy density but low total thermal energy. Fig 2b shows the bonded CNT-NF interface. The thermal boundary resistance is again measured after bonding ("bonded" data).

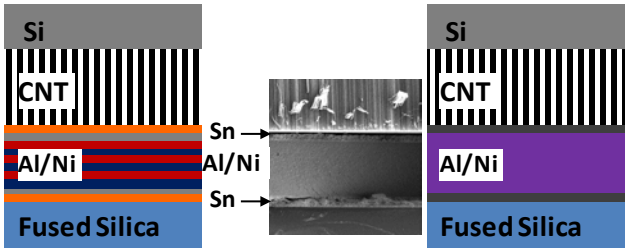

(a) (b) (c)

Fig. 3: (a) Schematic of CNT-Nanofoil-FS interface before alloying. The NF layer begins as a Sn-plated Al/Ni superlattice placed between the two adjacent metalized surfaces. (b) SEM of CNT-NF-FS interface after bonding. High resolution microscopy verifies the quality of the mechanical contact at the Sn-Au interface and allows for observation of any potential damage to the CNT film during compression and bonding. (c) Schematic of CNT-NF-FS interface after alloying. The Al/Ni alloy remains after bonding but contributes minimally to the total thermal interface resistance between the CNT film and the substrate. Since this metallic alloy has a thermal conductivity of ~35 W/m/K [16], the thermal resistance of this layer is expected to be small relative to the Sn-Au interfaces.

Infrared Thermometry

The thermal conductivity of the CNT films and CNT-substrate interface resistances are measured using comparative infrared (IR) microscopy [8]. The IR microscope generates a high-resolution, two-dimensional temperature profile with a spatial resolution of 2 μm and a temperature resolution of 0.1K. An advantage of this technique is the ability to independently extract the bulk thermal conductivity of the CNT film and the thermal boundary resistances before and after bonding.

The CNT films are bonded to fused silica substrates, which are also used as reference layers for the thermal measurements. Fused silica is chosen as reference layer because it has a stable thermal conductivity over a wide range of temperatures ($k_{\text{fused silica}}$ = 1.4 W/m/K). The sample stack (silicon-CNT-fused silica) is then placed between a heat source and a heat sink. The bulk CNT film is also characterized by placing it in dry contact with metalized fused silica without any bonding layer. Each layer in the stack has the same cross-sectional area, which enables the use of a one-dimensional heat conduction model. Convection and radiation losses are neglected in the analysis because they are small compared to the conduction through the CNT interface. A second reference layer is placed on the other side of the stack to quantify these heat losses by comparing the heat flux conducted through the each reference layer. The magnitude of the heat flux through the CNT film is bounded by the heat flux measured at each reference layer.

The heat flux q'' through each layer in the measurement stack can be calculated with Fourier's Law:

$$q'' = -k\frac{dT}{dx}, \tag{1}$$

where k is the thermal conductivity of the layer and dT/dx is the temperature gradient in the layer.

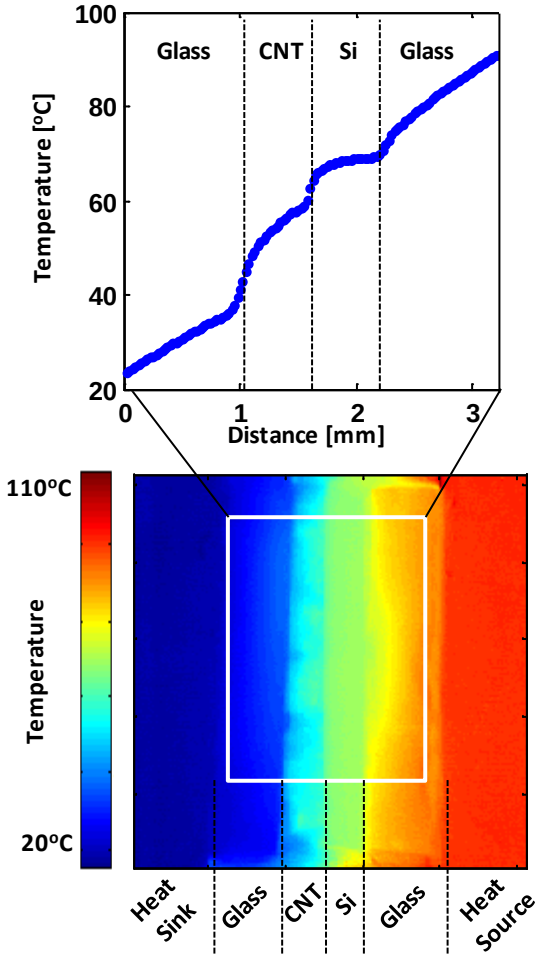

Fig. 4: (top) Averaged temperature profile across a sample stack (fused silica-CNT-Si-fused silica) placed between a heat sink and heat source. (bottom) Two-dimensional temperature map of the CNT configuration. Each column of temperatures within the white square marked in (b) is averaged to yield the temperature profile shown in (a). The white square is selected in the center of the stack to avoid convective edge effects. Nonlinearities in the silicon and CNT temperature profile near the interface are due to boundary effects and surface roughness and are not considered when calculating the thermal conductivity of the CNT film.

After reaching steady state, the temperature profile across the stack is measured using IR microscopy. The thermal conductivity of the CNT film is calculated by comparing the temperature gradient in the reference layer to the temperature gradient of the bulk CNT film, as in Eq. 2.

$$\frac{k_{sample}}{k_{reference}} = \frac{\left(\frac{dT}{dx}\right)_{reference}}{\left(\frac{dT}{dx}\right)_{sample}} \tag{2}$$

The thermal boundary resistance R'' across an interface is computed by comparing the interfacial temperature drop to the heat flux conducting through the sample,

$$R'' = \frac{\Delta T_{int}}{q''} = \frac{\Delta T_{int}}{k_{ref}\left.\frac{dT}{dx}\right|_{ref}} \quad (3)$$

where ΔT_{int} is the interfacial temperature drop.

An apparatus was constructed with three orthogonal linear stages to allow precision alignment and control of compressive strain on the sample stack under the IR microscope. This rig provides a maximum hot-side temperature of 180°C and a minimum cold-side temperature of 5°C. Pressure across the stack is measured using a load cell (Omega LCMKD-10N) affixed in series to the micrometer actuator controlling the compressive axial strain.

The two-dimensional IR temperature measurements are reduced to a one-dimensional temperature profile by taking the mean temperature of each cross-section perpendicular to the direction of the heat flow. This yields a linear temperature profile across each layer of the sample as shown in Figure 4. A least-squares linear fit is applied to compute the temperature gradient in each layer. The thermal boundary resistance at the CNT-fused silica interface can be found by measuring the temperature drop across the interface and applying Eq. 3. To improve the accuracy of this calculation, data are taken over a range of applied heat fluxes. The thermal conductivity is then calculated from the slope of a heat flux as a function of the temperature gradient in the CNT layer, $dT/dx|_{CNT}$. Similarly, the thermal boundary resistance is computed from the slope of the interfacial temperature jump $\Delta T|_{int}$ as a function of the applied heat flux.

CNT Film Transfer

The goal of bonding is to provide a thermal conduction pathway across the interface as well as to mechanically attach the CNT film to the device. The mechanical adhesion of the bond is stronger than the van der Waals forces at the growth interface, and therefore the silicon growth substrate can be removed (see Figure 5). The newly exposed CNT surface can then be metalized and bonded to a second surface. This procedure enables the integration of a CNT TIM between a heat source and a heat sink. This completes the bonding and transfer of a CNT film from a growth substrate to an application device.

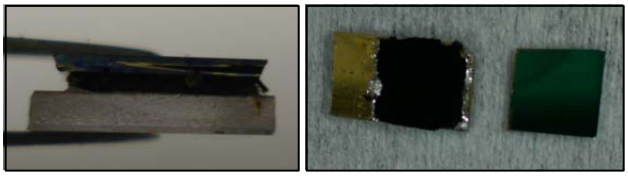

(a) (b)

Fig. 5: (a) CNT film is bonded to a fused silica substrate with original growth silicon substrate still attached. (b) Since the indium and NF bonds are stronger than the CNT adhesion to the growth substrate, the silicon can be pulled away.

RESULTS

Figure 6a shows measurements of the bulk CNT film conductivity with dry contacts. The error bars denote the upper and lower bounds on thermal conductivity based on the bounds of the applied heat flux as measured by the two reference layers. k_{CNT} may initially increases with pressure because more CNTs come into contact with the surface and participate in conduction. k_{CNT} then reaches a plateau as the sample is further compressed and all of the CNTs become engaged in thermal conduction. Figure 6b shows a decreasing trend in thermal boundary resistance with pressure for un-bonded (dry contact) CNT films, indicative of increased contact between the CNTs and the fused silica substrate. These values are used as the baseline for comparing improvements in TIM performance with metallic bonding. A sharp temperature jump at the interface is evident between the CNT film and the metalized fused silica without a bonding layer, and the temperature jump at the interface is significantly reduced when a solder bonding technique is utilized, which is demonstrated in Figure 7.

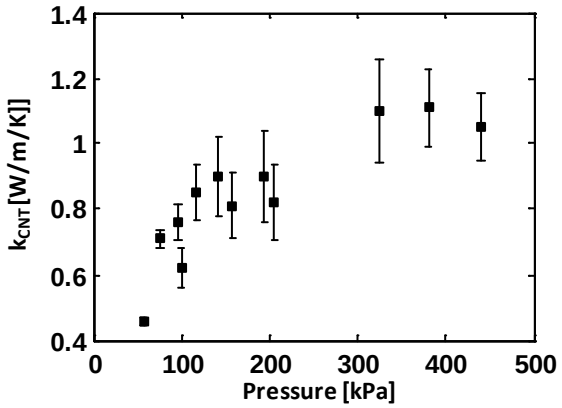

(a)

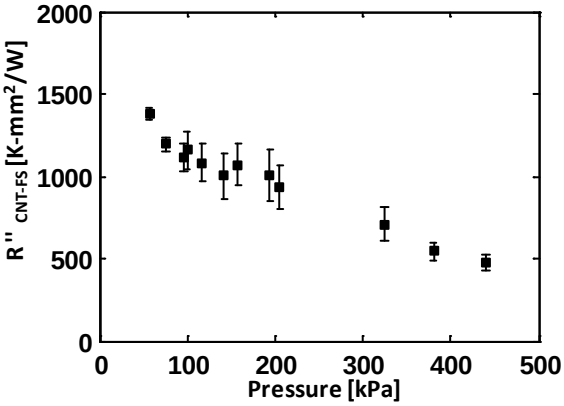

(b)

Fig. 6: (a) Thermal conductivity of a CNT film as a function of applied pressure for unbonded CNT films in contact with metalized fused silica substrates. (b) Thermal boundary resistance of CNT-fused silica interface without any bonding layers. This resistance represents the upper bound for the CNT-fused silica interface since it represents dry contact.

After indium bonding, the thermal boundary resistance is measured over a range of applied pressures. The indium film has a thermal conductivity of k_{indium} ~ 80 W/m/K and does not contribute significantly to the thermal resistance of the interface (~0.3 mm^{2}K/W). The quality of the CNT-In-FS bond depends strongly on how well the indium wets the CNT film and the substrate. The CNT-In-FS thermal boundary resistance $R''_{CNT\text{-}In\text{-}FS}$ is measured to be 28-71 mm^{2}K/W which varies

with pressure. Figure 8a shows that the unbonded interface exhibits decreasing resistance with pressure, and after bonding with indium, increasing pressure does not significantly impact the thermal boundary resistance. This pressure independence is characteristic of a good metallic bond. The unbonded interface resistance is approximately R" = 10^3 K-mm^2/W and does not depend on the type of metal bonding layer present.

NF bonding is performed *in situ* under the IR microscope and the temperature profile is obtained before and after the bonding reaction. This isolates the effect of the bond itself on interface resistance. As seen in Figure 7, a NF-bonded interface dramatically reduces the temperature jump between the two contacting surfaces. Figure 7 shows that for the same applied heat flux (as indicated by the temperature gradient in the FS), the total temperature drop across the interface is substantially reduced after bonding.

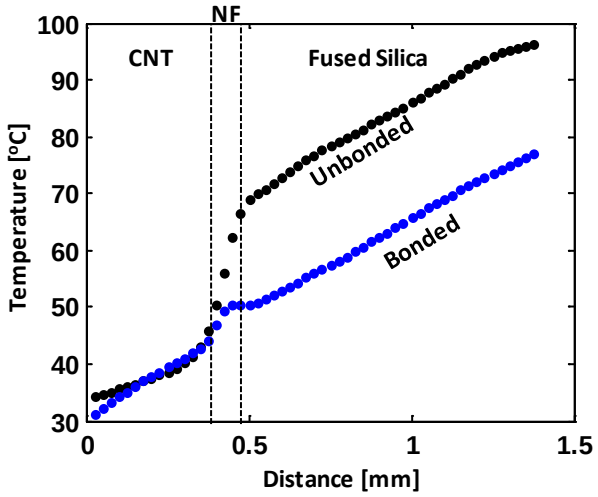

Fig. 7: Comparison of interface temperature drop across a NF bonding layer before and after bonding. Since the temperature drop is reduced, the maximum temperature on the hot side is lower after bonding.

Figure 8b shows that the CNT-NF-FS thermal boundary resistance, $R''_{CNT\text{-}NF\text{-}FS}$, after NF bonding is 15-50 mm^{2}K/W. The principal component of this resistance is at the Sn-Au interfaces and not the bulk NF bonding layer. Figures 8a and 8b show that the thermal resistance value monotonically decreases with pressure up to 500 kPa. Preliminary tests have verified the stability of NF bonding under thermal cycling conditions up to 500°C under vacuum.

After compressive axial strain is applied to the system, viscoelastic effects are observed as the system reaches mechanical equilibrium [2, 17, 18]. The compressive stress initially increases rapidly with the application of compressive strain. At constant strain, the stress decays exponentially with time as the CNT film relaxes to a steady state value. Thermal expansion in conjunction with the fixed strain condition leads to increasing pressure while varying the heat flux for each measurement. The pressure is permitted to reach a steady value at each measurement interval. Figure 9 shows a characteristic stress relation curve illustrating this viscoelastic effect.

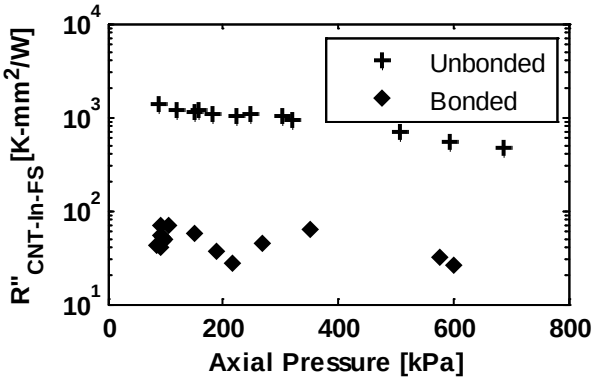

(a)

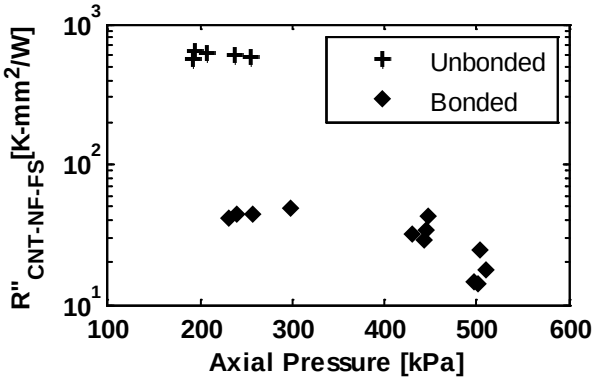

(b)

Fig. 8: Comparison of un-bonded and bonded CNT-fused silica interface resistance using (a) indium bonding layer and (b) NF bonding layer. The unbonded NF data was only taken up to 260 kPa. The thermal boundary resistance for the NF bond exhibits a dependence on applied compressive pressure.

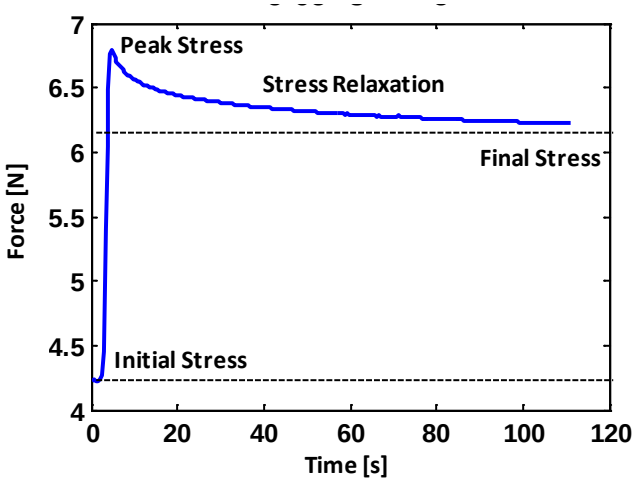

Fig. 9: Viscoelastic stress relaxation of CNT film under constant axial strain. A compressive strain is applied to the film, raising the stress from an initial state to a peak state. Under constant strain, the CNT film relaxes from its peak stress to a final steady state value.

Deck *et al.* [18] proposed using a Maxwell model typically used to model polymer deformation for the time-dependent stress relaxation in a CNT film:

$$\sigma(t) = \sigma_0 e^{-t/\tau} + \sigma_{final}, \quad (4)$$

where σ_o is an amplitude fitting parameter, σ_{final} is the steady state stress value, and τ is the stress relaxation time constant. Measured stress relaxation curves are fit with a Maxwell model (see Figure 10) to characterize the viscoelastic response of the CNT film under axial compression. During each successive compression, the average time constant was found to be τ = 19.2 s.

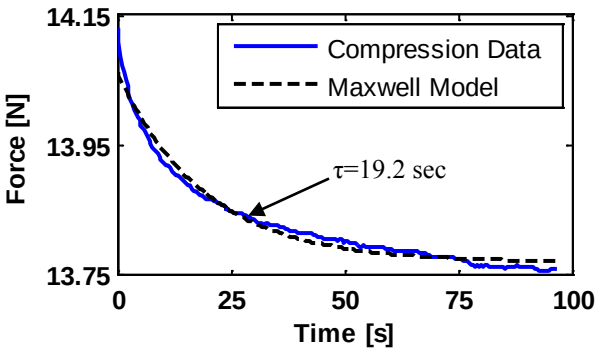

Fig. 10: Stress relaxation curve and corresponding Maxwell model fit. The Maxwell model is adapted to CNT films, which exhibit viscoelastic behavior similar to polymers.

SUMMARY AND CONCLUDING REMARKS

We use two bonding methods to reduce the thermal interface resistance between CNT films and surrounding materials. Low temperature solder bonding, with a thin indium foil, reduces the interface resistance from the unbonded case of ~1000 mm^2K/W to ~50 mm^2K/W. Indium shows potential for low temperature (<160°C) thermal interface applications, such as cooling systems in computers. For other applications, Nanofoil bonding provides the thermal conductance of a soldered interface with high-temperature stability. Specifically, the thermal boundary resistance of a NF bond was found to be slightly better than a comparable indium bond. Since NF bonding is a solid-solid welding reaction, we achieve a solder bond that does not suffer from performance degradation at high operating temperatures (<1000°C) due to phase change limitations of the solder bonding layer.

Both indium and NF are thermally conductive and easy to integrate as a bonding layer for nanostructured TIMs. In both cases, the CNT film and target substrate are first metalized and the indium or Nanofoil creates a direct bond between the CNT film and the target substrate (*i.e.* heat sink assembly). These techniques preserve the mechanical compliance and high intrinsic thermal conductivity of the CNT-based TIM and significantly improve the thermal boundary resistances at TIM-substrate interfaces. Future work will integrate NF and indium to develop a freestanding CNT-based tape design TIM that is scalable and easy to integrate into thermal interface applications [19]. The thermal and mechanical performance of this TIM will be studied in anticipated device operating conditions, including rapid temperature fluctuations, large temperature gradients, and a large number of thermal cycles.

ACKNOWLEDGEMENTS

The authors gratefully acknowledge financial support from the NSF/DOE Partnership on Thermoelectric Devices for Vehicle Applications (Grant No. 1048796), the National Science Foundation Graduate Research Fellowship program, and the Stanford Graduate Fellowship program. This work was also supported by the Office of Naval Research ONR (N00014-09-1-0296-P00004, Dr. Mark Spector, program manager).

REFERENCES

[1] E. Pop, *et al.*, "Thermal Conductance of an Individual Single-Wall Carbon Nanotube above Room Temperature," *Nano Letters*, vol. 6, pp. 96-100, 2006.

[2] Y. Won, *et al.*, "Mechanical characterization of aligned multi-walled carbon nanotube films using microfabricated resonators," *Carbon*, vol. 50, pp. 347-355, 2012.

[3] Y. Gao, *et al.*, "Nanostructured Interfaces for Thermoelectrics," *Journal of Electronic Materials*, vol. 39, pp. 1456-1462, 2010.

[4] S. V. Aradhya, *et al.*, "Electrothermally bonded carbon nanotube interfaces," in *Thermal and Thermomechanical Phenomena in Electronic Systems, 2008. ITHERM 2008. 11th Intersociety Conference on*, 2008, pp. 1071-1077.

[5] T. Tong, *et al.*, "Dense Vertically Aligned Multiwalled Carbon Nanotube Arrays as Thermal Interface Materials," *Components and Packaging Technologies, IEEE Transactions on*, vol. 30, pp. 92-100, 2007.

[6] X. Wang, *et al.*, "Noncontact thermal characterization of multiwall carbon nanotubes," *Journal of Applied Physics*, vol. 97, p. 064302, 2005.

[7] M. A. Panzer, *et al.*, "Thermal Properties of Metal-Coated Vertically Aligned Single-Wall Nanotube Arrays," *Journal of Heat Transfer*, vol. 130, p. 052401, 2008.

[8] A. M. Marconnet, *et al.*, "Thermal Conduction in Aligned Carbon Nanotube-Polymer Nanocomposites with High Packing Density," *ACS Nano*, pp. 4818-4825, 2011.

[9] S. R. Bakshi, *et al.*, "Carbon nanotube reinforced metal matrix composites - a review," *International Materials Reviews*, vol. 55, pp. 41-64, 2010.

[10] R. Andrews, *et al.*, "Purification and Structural Annealing of Multiwalled Carbon Nanotubes at Graphitization Temperatures," *Carbon*, vol. 39, pp. 1681-1687, 2001.

[11] S. L. Hodson, *et al.*, "Palladium Thiolate Bonding of Carbon Nanotube Thermal Interfaces," *Journal of Electronic Packaging*, vol. 133, p. 020907, 2011.

[12] A. Hamdan, *et al.*, "Evaluation of a thermal interface material fabricated using thermocompression bonding of carbon nanotube turf," *Nanotechnology*, vol. 21, p. 015702, Jan 8 2010.

[13] R. D. Johnson, *et al.*, "Thermocompression bonding of vertically aligned carbon nanotube turfs to

metalized substrates," *Nanotechnology*, vol. 20, p. 065703, Feb 11 2009.

[14] R. Cross, *et al.*, "A metallization and bonding approach for high performance carbon nanotube thermal interface materials," *Nanotechnology*, vol. 21, p. 445705, Nov 5 2010.

[15] S. S. Too, *et al.*, "Indium thermal interface material development for microprocessors," in *Semiconductor Thermal Measurement and Management Symposium, 2009. SEMI-THERM 2009. 25th Annual IEEE*, 2009, pp. 186-192.

[16] *http://www.indium.com/nanofoil/*.

[17] Q. Zhang, *et al.*, "Viscoelastic creep of vertically aligned carbon nanotubes," *Journal of Physics D: Applied Physics*, vol. 43, p. 315401, 2010.

[18] C. P. Deck, *et al.*, "Mechanical behavior of ultralong multiwalled carbon nanotube mats," *Journal of Applied Physics*, vol. 101, p. 023512, 2007.

[19] M. A. Panzer, *et al.*, "Composite Thermal Interface Material Including Aligned Nanofiber with Low Melting Temperature Binder 2009/0068387A1," United States Patent, 2007.